Proceedings World Geothermal Congress 2010
Bali, Indonesia, 25-29 April 2010

Interpreted Fracture Anomalies: Joint Imaging of Geophysical Signals from Fluid-Filled Fracture Zones in Geothermal Fields

Stephen Onacha, Eylon Shalev, Peter Malin, Peter Leary and Lake Bookman

Institute of Earth Science and Engineering, Auckland University, Level 6, 58 Symonds Street, Private Bag 92019, Auckland 1142, New Zealand

s.onacha@auckland.ac.nz

Keywords: Geophysical exploration, aligned fracture zones, heterogeneity, anisotropy, S-wave splitting, polarization

ABSTRACT

We present the theory and application of a joint imaging and interpretation approach to seismic shear-wave splitting and electrical resistivity polarization due to aligned, fluid-filled fracture zones. Previously, we have developed and tested methods for joint geophysical imaging (JGI) and interpretation of seismic velocity and electrical conductivity. The methods included coupling of physical properties as well as geological structures.

Our examples come from microearthquake (MEQ) recordings and magnetotelluric (MT) soundings in geothermal fields in Kenya and Iceland. We find that two main polarization directions align with both younger fractures and tectonically activated older fracture systems. The complex interconnection between these fracture zones causes heterogeneity and anisotropy, which determines fluid movement. As such, our field data and their joint interpretation have been used to successfully target geothermal exploration and production wells.

Our experience suggests that the best targets for drilling geothermal production wells are found along fracture zones that are aligned with tectonically activated fractures. Intersections of different trending fractures also form important fluid up-flow channels. The alignment of fractures can be used to successfully drill high production wells. Due to heterogeneity and anisotropy, it is difficult to determine and predict fluid flow pathways and therefore routinely drilling across interpreted surface fractures does not always guarantee success. In our Kenyan example, the most successful wells in a new field were targeted along NW trending fractures which form a zone of enhanced permeability. A similar result was found in the Icelandic example. From these cases we have concluded that the remedy for finding successful drilling targets is to focus on understanding the heterogeneity and anisotropy at depth, an instance of which is the joint-imaging methods described here.

1. INTRODUCTION

The quest for new geothermal fields and increasing productivity from existing fields has intensified worldwide. The biggest challenge has been and remains the ability to successfully target and drill high production wells that could significantly lower the costs, and time required to bring geothermal energy into production. This paper presents some of the results of successful well targeting using a JGI scheme of MEQ from new data loggers and co-located MT measurements. The focus of the JGI approach is to locate high permeability zones as targets for drilling. We have used S-wave splitting and MT polarization as a measure of anisotropy caused by fluid-filled fractures. S-wave tomography is routinely carried out assuming one dominate polarization direction. Due to heterogeneity and anisotropy caused by aligned fluid-filled fractures, the assumption for one dominant polarization direction might not be entirely valid. The joint interpretation of resistivity and MEQ data can be carried out by using a basis function to solve a modified double porosity model by Flovenz et al., (1995), Onacha (2006), Onacha et al., (2007).

$$\frac{1}{\rho} = \frac{0.22}{\rho_w}\left[1-\left(1-\Phi\right)^{\frac{2}{3}} + \frac{\left(1-\Phi\right)^{\frac{2}{3}}}{1+\left(1-\Phi\right)^{\frac{1}{3}} * 4.9 * 10^{-3}}\right]\frac{\Phi^{1.2}}{\mathrm{b}} \quad (1)$$

Where Φ is porosity, ρ is the resistivity, ρ_w is the temperature dependent resistivity of the water, and b is a temperature related constant which is determined empirically. The resistivity of the geothermal water can be determined from either laboratory measurements or the total dissolved solids in the geothermal fluids.

2. BRIEF THEORY AND SYTHETIC MODELS

2.1 The porosity and resistivity relationship

The solution of equation 1 above using a basis function yields a log-log distribution porosity-resistivity relationship (Figure 1) as shown below. The porosity-resistivity relationship shows that when the interpreted resistivity is above 130 Ωm, then the porosity is very low.

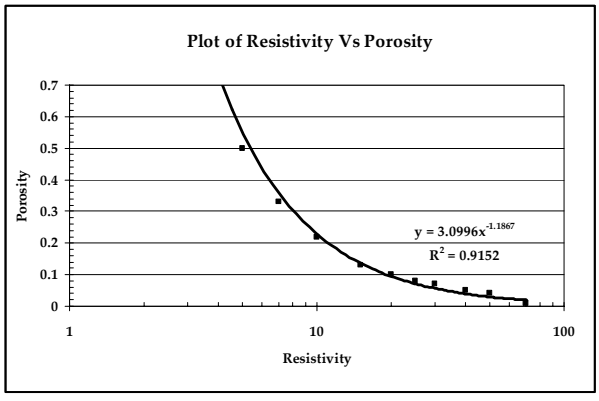

Figure 1: Plot of resistivity against porosity derived from solving a basis function for a double porosity model relating porosity to resistivity close to the fracture zone.

The relationship between porosity and resistivity is given in the formula shown below:

$$\text{Log } \Phi = \log M - 1.2 \log \rho \quad (2)$$

Where Φ is porosity, M is a constant between 2.5 and 3.5 and ρ is resistivity.

2.2 The relationship between porosity and bulk velocity

The P-wave velocity and porosity relationship has been established based on the equation by Wyllie et al., 1958 as shown below:

$$\frac{1}{V_p} = \frac{\Phi}{V_w} + \frac{1-\Phi}{V_r} \tag{3}$$

Where V_p is the bulk P-wave velocity, V_w is P-wave velocity of water, V_r is the P-wave velocity of the rock and Φ is the porosity. In our analysis, we assume that fractured geothermal reservoirs are mainly controlled by fracture porosity. If the P-wave velocity of water and the reservoir rock P-wave velocity are known, then porosity can be determined from the measured bulk P-wave velocity from tomography or direct laboratory measurements from well cores. In Iceland, P-wave velocity for basalts determined from cores by Christensen and Wilkins (1982) is 6250ms^{-1} and the P-wave velocity of water is about 1500ms^{-1}.

This relationship together with the Wyllie equation was used to establish the empirical relationship between porosity and P-wave velocity as shown below:

$$\Phi = 1974 ms^{-1} V_p^{-1} - 0.32 \tag{4}$$

Based on the assumption that both the bulk P-Wave velocity and resistivity in the geothermal reservoir are affected by fracture porosity, equations 1 to 4 can be used for joint imaging of high permeability fracture zones. From a starting velocity model, the porosity operator, we can generate synthetic models. From the analysis of the relationship between resistivity and porosity, this study assumes that in areas with resistivity high than 130 Ωm the fracture porosity is very low and the P-wave velocity approaches that of the rock matrix. It is therefore expected that the variation in porosity will be significant only in areas with low resistivity close to the fracture zone.

The fluctuations in porosity are assumed to be proportional to the fluctuations in the log of permeability. The link between resistivity, P-wave velocity and porosity is defined through a porosity-operator Onacha et. al., (2007) such that

$$f(\Phi_f) = \begin{Bmatrix} 0 & \rho \geq 130 \Omega m & V_p \geq 6250 ms^{-1} \\ 0.5-0\cdots 5 \geq \rho \leq 130 \Omega m \ldots & & 2500 \geq V_p \leq 6250 ms^{-1} \\ 1-0.5 & 0 \geq \rho \leq 5 \Omega m & V_p \leq 2500 ms^{-1} \end{Bmatrix} \tag{5}$$

We further make a piece wish function from the porosity operator which is then used in deriving porosity from either the resistivity or from the velocity model.

2.3 Synthetic 2D velocity, resistivity and porosity

We generated resistivity and porosity from synthetic velocity models which incorporate velocity fluctuations about a mean (1/f noise) Leary et. al., (2009). The details of the velocity model including a low velocity vertical narrow anomaly that depicts a fracture zone and a step resistivity contrast depicting a fault scarp are reproduced in the synthetic resistivity and porosity models using equations 2 to 5 above. From the analysis of the synthetic models, the structural complexity and boundary relationships are preserved in the synthetic porosity and resistivity models. The porosity relationship between resistivity and P-wave velocity can therefore be used to determine areas of enhanced permeability in fractured reservoirs. The porosity relationship can be used for a joint MT and MEQ imaging scheme that assumes fluctuations in P-wave velocity are proportional to fluctuations in the log of resistivity Malin et. al., (2009).

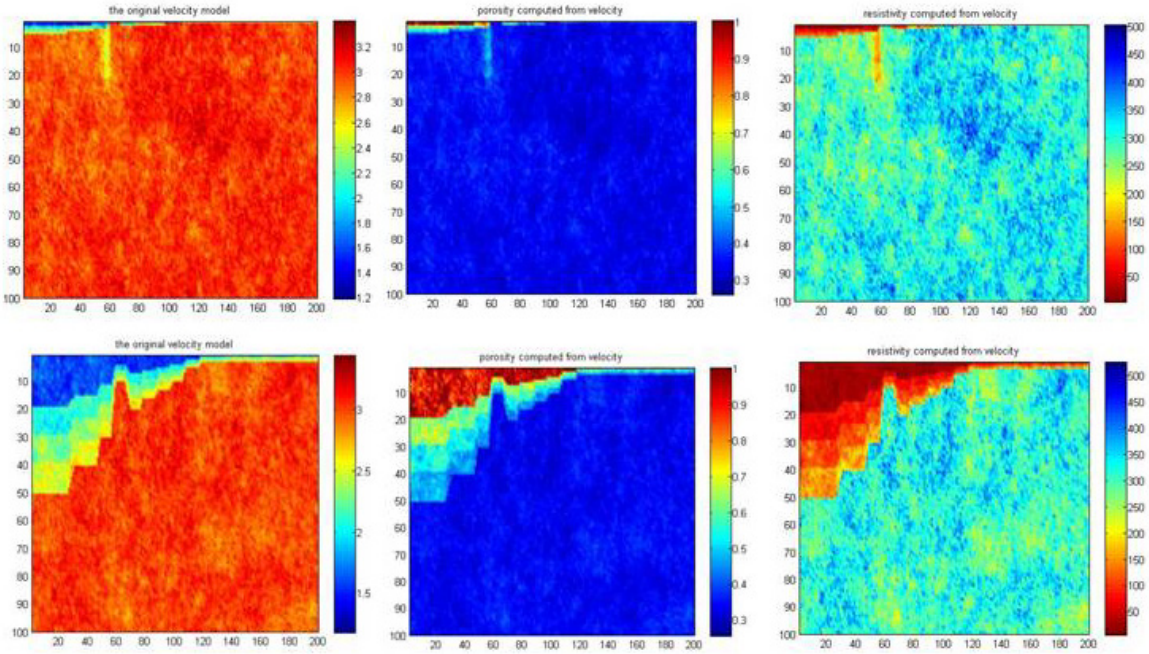

Figure 2: Synthetic 2D models for 100x200 grid velocity models (left panels), synthetic porosity models (middle panels) and synthetic resistivity models (right panels).

2.4 S-wave splitting and MT polarization

S-wave splitting is a diagnostic and measurable property of seismic anisotropy which is caused by fluid-filled, stress aligned cracks, Crampin and Peacook (2005). S-wave splitting was done by finding the angle that maximizes the amplitude ratio of the horizontal components of the S-waves. After rotating the S-waves to the directions parallel and perpendicular to this angle, the time delay between the slow and fast S-waves was found by cross-correlation of the amplitudes. The MT polarization at co-located sites with MEQ was found after rotated the MT impedance tensor to the principal directions. The S-wave splitting time delays are compared to splitting in the MT data while the direction of the fast S-wave is compared to the polarization in the MT data. From the results of wells drilled using a combination of S-wave splitting and MT polarization, it is evident that these results can be used to understand heterogeneity and anisotropy which can be used to determine fluid-filled fractures as targets for drilling. This would be a preferred approach rather than routinely drilling across traces of surface structures.

The MT data was analyzed by determining a measure of splitting at each frequency by computing the percentage difference (f) = (logrhomax(f))-logrhomin(f)) / logrhomin(f). This gives a measure of anisotropy at each frequency less than 0.01Hz. A splitting max-threshold and min-threshold is set such that when the percentage difference is above the max-threshold, then splitting is assumed to have occurred and data is then counted backwards until the splitting is below the defined minimum threshold set at a variable percent of the max-threshold.

This approach has been used to pick the frequency at which splitting occurs and the amount of frequency dependent splitting as a measure of anisotropy. The frequency at which the splitting occurs in data acquired in Olkaria, Kenya (Figure 3) was used to determine the depth at which splitting occurs. The splitting is frequency dependent probably indicating the spatial variation in anisotropy due to fluid-filled fractures. This splitting occurs in different areas irrespective of the local geology. An example of splitting in the MT data from the Krafla geothermal field in Iceland is given below (Figure 4). When MT data is interpreted on its own, the splitting is sometimes attributed to near surface conductance anomalies that scatter the electric fields, Simpson and Bahr (2005). In this paper, we infer that the splitting in most geothermal fields is attributed to the effect of fluid-filled fractures. This assumption is supported by S-wave splitting at the same sites as the MT data. This approach demonstrates the value of using both MT and MEQ to located fluid-filled fractures

2.5 Location of MEQ

The MEQ data used were acquired from 6 down hole seismometers in the Krafla geothermal field in Iceland. 5 seismometers were deployed in 2006 and 1 more deployed in 2008. The location of MEQ was done using Hypoinverse code, Klein (2002) using a velocity model derived from resistivity, Onacha (2006). The MEQ data recorded between August 2006 and July 2008 were relocated using the double difference algorithm of Waldhauser (2002). The results shown in this paper used only catalog type data and the next phase will use cross correlation of the amplitudes to improve on the location of clusters of repeating earthquakes that might be correlated to structures or geothermal activity like re-injection and well discharge. The MEQ locations obtained by using the double difference are similar to those obtained using the Hypoinverse code. The absolute location of the earthquake cluster has not been adjusted, it is hoped that in the future this will be achieved.

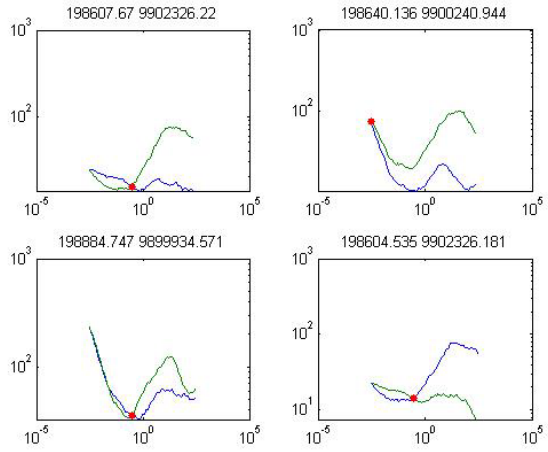

Figure 3: Examples of MT data from Olkaria, Kenya showing the frequency (indicated by a red filled circle) at which splitting occurs. The splitting occurs is indicative of the spatial variation in anisotropy probably due to fluid-filled fractures.

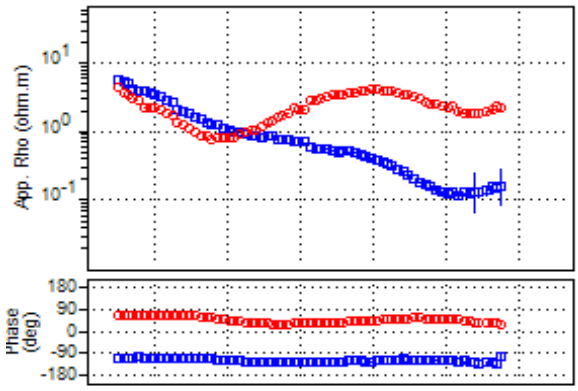

Figure 4: Principal apparent resistivities and impedance phases from an MT site close to an interpreted fluid-filled fracture at Krafla, Iceland

2.6 Joint Geophysical Imaging of MEQ and MT data

The first stage of the JGI for MEQ and MT data is to achieve by separate 2D inversion of MT after joint interpretation with Transient Electromagnetic (TEM) and tomography of MEQ data. The results of this stage are then converted to porosity models using a similar approach to that used to obtain the synthetic models as described in section 2.3 above. Weighted inversion schemes for both the porosity obtained from MEQ and MT were used to obtain a porosity distribution that is indicative of the permeability distribution in the fractured geothermal reservoir. This is based on the observations of well-core small scale porosity-permeability fluctuation relationship which shows that the fluctuation in porosity is proportional to the fluctuation in the log of porosity, Leary and Malin (2009).

3. RESULTS

3.1 Location of MEQ

The location of MEQ using velocity models computed from resistivity both in Kenya and Iceland indicate that MEQ

locations are controlled mainly by NW and NE trending linear alignments which are probably related to deep older re-activated fractures and younger active fractures. For the case of Krafla and Olkaria, the NS trending fractures associated with rifting do not seem control the location of MEQ except in the vicinity of the major NW trending structures. This is important in terms of determining which fractures to target for enhanced permeability. The location of MEQ (Figure 5) from the 6 down hole shows a clustering of earthquakes in the geothermal field associated with production and re-injection in the field and fluid-movement along fractures. This network also demonstrates the importance of a dedicated monitoring system that can also be used to guide development in an existing field.

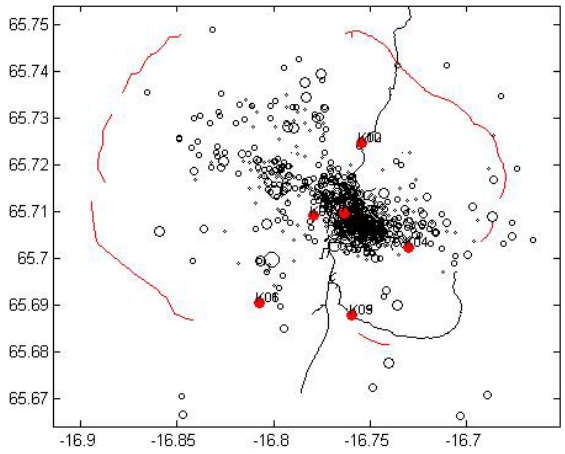

Figure 5: Location of MEQ at the Krafla geothermal field. The location of the down hole seismometers are shown in red filled circles.

The MEQ location from double difference shows a similar trend to the from Hypoinverse location (Figure 6). The double difference locations are for data recorded from August 2006 and August 2008. The clustering of the earthquakes in a SE trend probably shows the boundaries of the geothermal system. The analysis of cross sections of projected MEQ locations in the NW and NE indicates that MEQ do not occur below a depth of 4-5Km. This probably marks the region of transition to partial melt that provides the heat source for the geothermal system in Krafla.

3.2 P-wave seismic tomography

The results of P-wave tomography at the Krafla geothermal field where we recorded over 2,500 events show very few ray hits at a depth of more than 3.5Km (Figure 7). The deeper earthquakes occur to the NW and NE of the geothermal field. The results of tomography at different depths slices (Figure 8) show that the northern part of the Krafla geothermal field is associated with a high Vp velocity. The high Vp velocity zone is associated with high resistivity.

3.3 S-wave splitting and MT polarization.

The results of S-wave splitting and MT polarization show that the combined use of these methods is an effective tool in determining a measure of anisotropy due to fluid-filled aligned fractures in geothermal system. We give an example of the application of these two methods to determine drilling directions for the most productive wells in the new Olkaria-Domes geothermal field in Kenya. In this example S-wave splitting and MT polarization are aligned mainly in the NW and NW directions (Figure 9). The successful wells were drilled to target the NW trending fractures which were interpreted as zones of enhanced permeability. The polarization directions together with an analysis of the amount of splitting in the MT data (Figure 10) as a proxy measure of anisotropy due in the vicinity of fluid-filled aligned fractures, were used to determine the best targets for drilling.

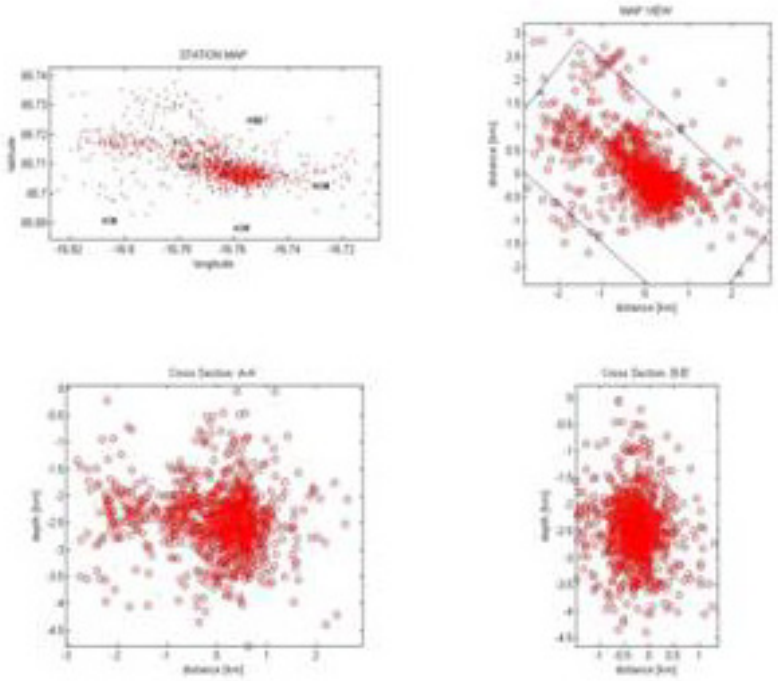

Figure 6: Location of MEQ at the Krafla geothermal field in Iceland from a network of down hole seismometers.

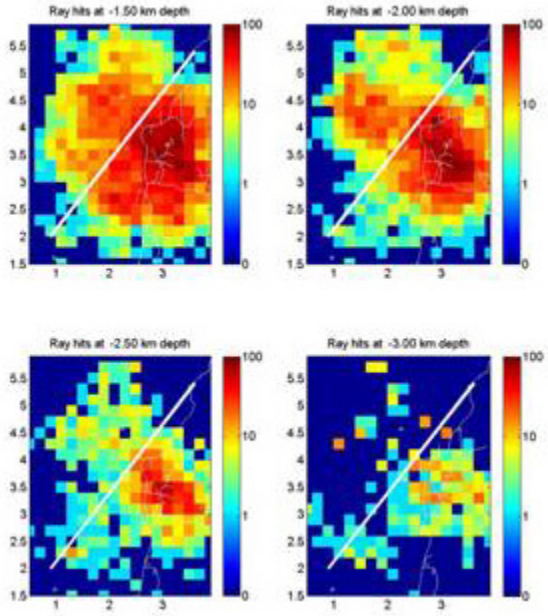

Figure 7: Ray hits at different depths slices from ray tracing. Deep MEQ locations are mainly on the edge of the geothermal field. The white line indicates the profile used for joint interpretation with resistivity data.

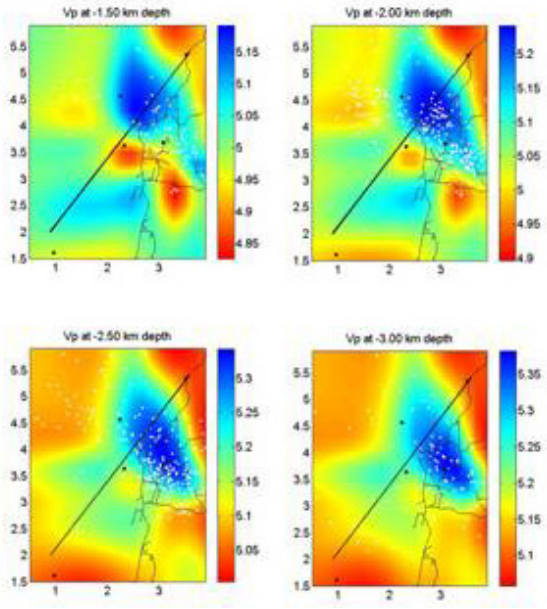

Figure 8: Results of Vp tomography at different depths slices at the Krafla geothermal field. The location of MEQ used for tomography are shown as white dots

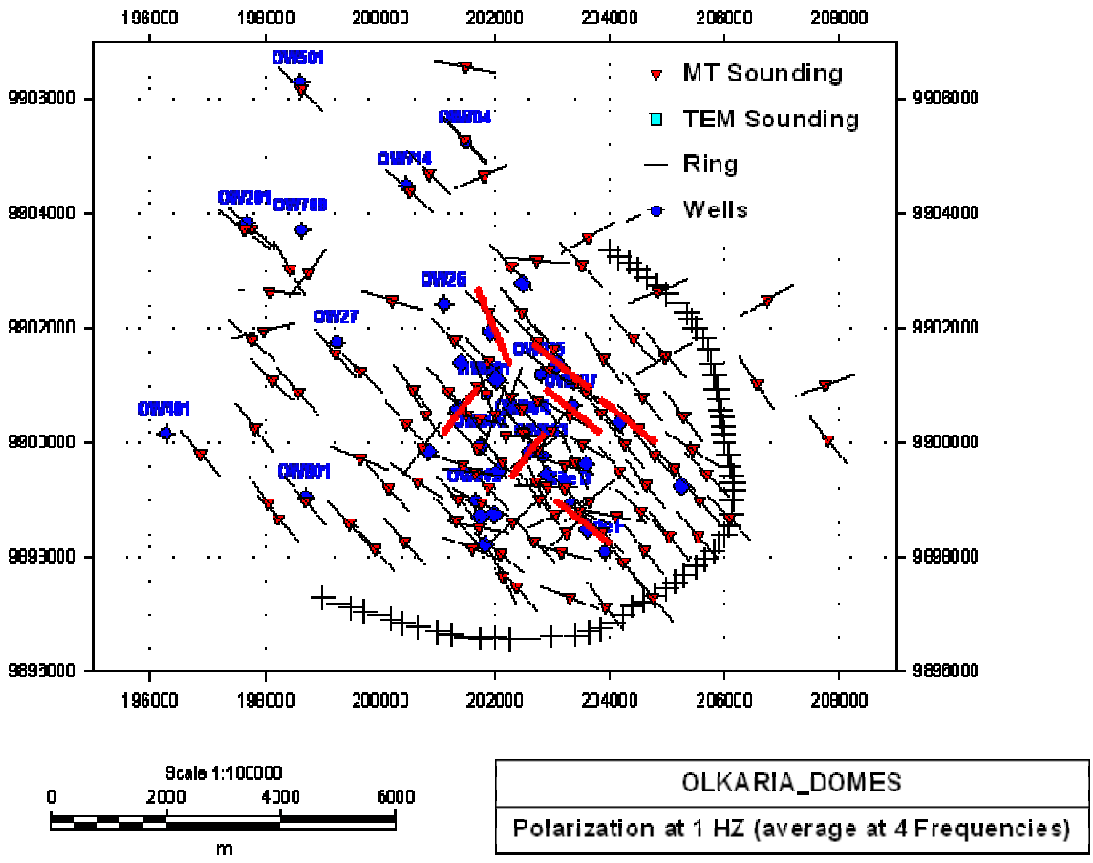

Figure 9: Map showing S-wave splitting and MT polarization directions for co-located MT and MEQ stations in the Olkaria-Domes geothermal field.

The results of the MT splitting should always be interpreted together with the types of the resistivity curves. Our experience shows that although some splitting may occur at the boundary of the geothermal, the most diagnostic evidence is the continuously increasing with depth e.g. around well OW801which may be attributed either to lower temperatures and lower fracture permeability.

This result indicates that electrical polarization and S-wave splitting respond to spatial variations in permeability in fractured geothermal fields Onacha (2009).

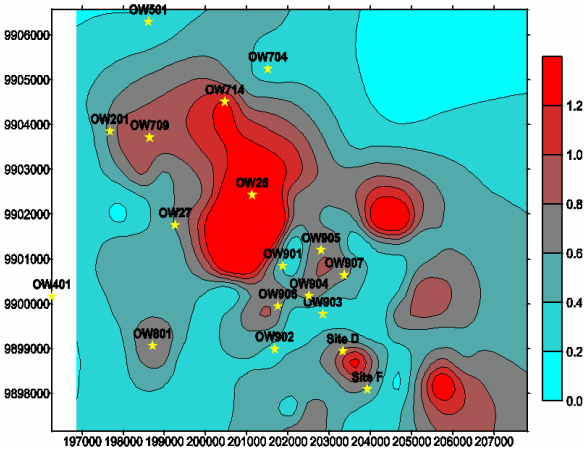

Figure 10: Map showing the maximum splitting of the MT data in the Olkaria-Domes area. The wells on the boundary of the field e.g. OW 501 and OW 704 are associated with low splitting in the MT data

3.4 Joint Geophysical Imaging (JGI).

The results from the studies of co-located MEQ and MT measurements show that locations of MEQ in high temperature geothermal systems in Kenya and Iceland are associated with boundaries of low resistivity and high resistivity anomalies. The map of the resistivity anomaly at 3000 meters below sea level (Figure 11) shows that the MEQ occur on the mainly on the boundary and above the deep low resistivity. The location of the MEQ defines a linear trend in the NW direction which is oblique to the clearly defined fracture swarms that have a NE trend. The caldera does also seem to determine the location of the MEQ. The association of the location of MEQ and resistivity boundaries is also evident at the Longonot geothermal field (Figure 12).

The relationship between porosity, P-wave velocity and resistivity were used to determine a poroperm distribution based on P-wave tomography and 2D MT data. The poroperm from both MEQ and MT data was derived by inversion using a mean weighted function that assumes that fluctuations in porosity are directly related to fluctuations in the log of permeability. As an initial step, the P-wave tomography section was converted to porosity. The MT 2D section was also converted to porosity. The weighted mean inversion scheme was then used to obtain a combined poroperm distribution (Figure 13) which indicates areas and depth as targets for drilling.

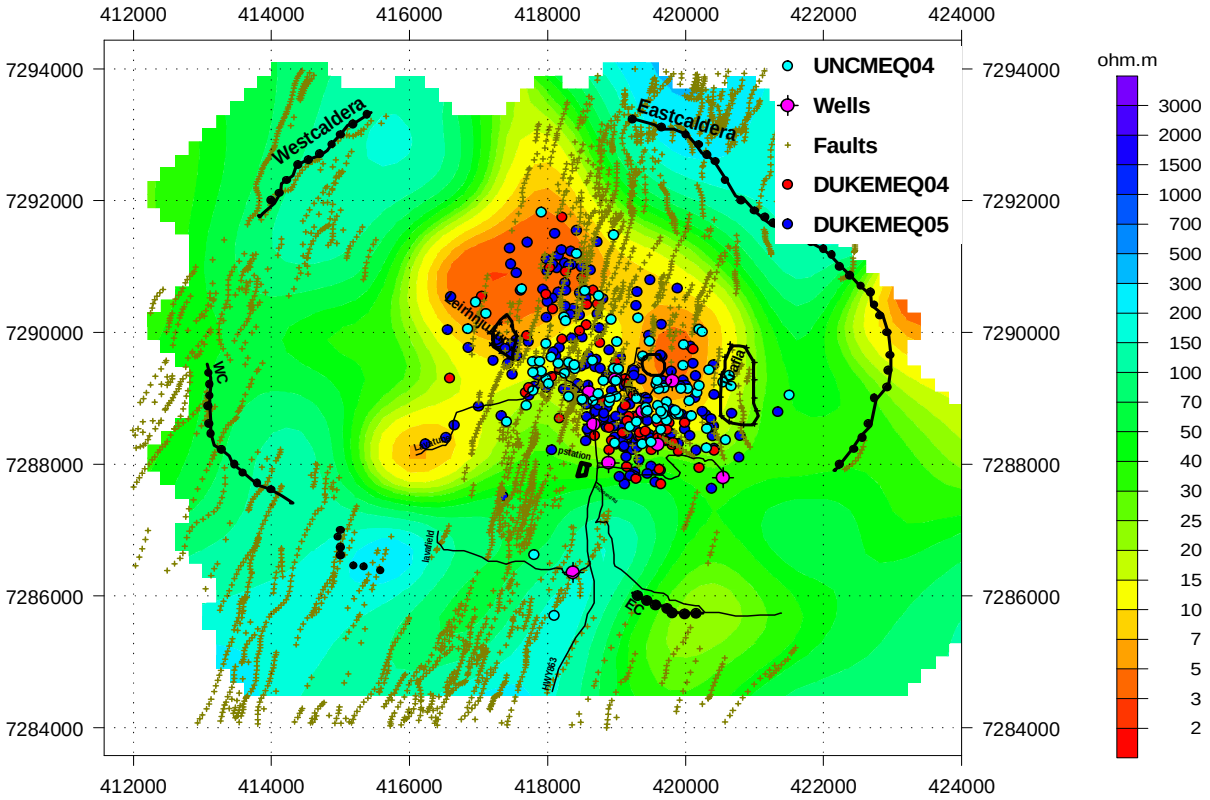

Figure 11: Resistivity map at an elevation of 2500 mbsl at the Krafla geothermal field in Iceland. The location of MEQ from data collected in 2004 and 2006 is also shown with deeper MEQ as blue filled circles. The surface fractures and the outline of the caldera boundary are also shown

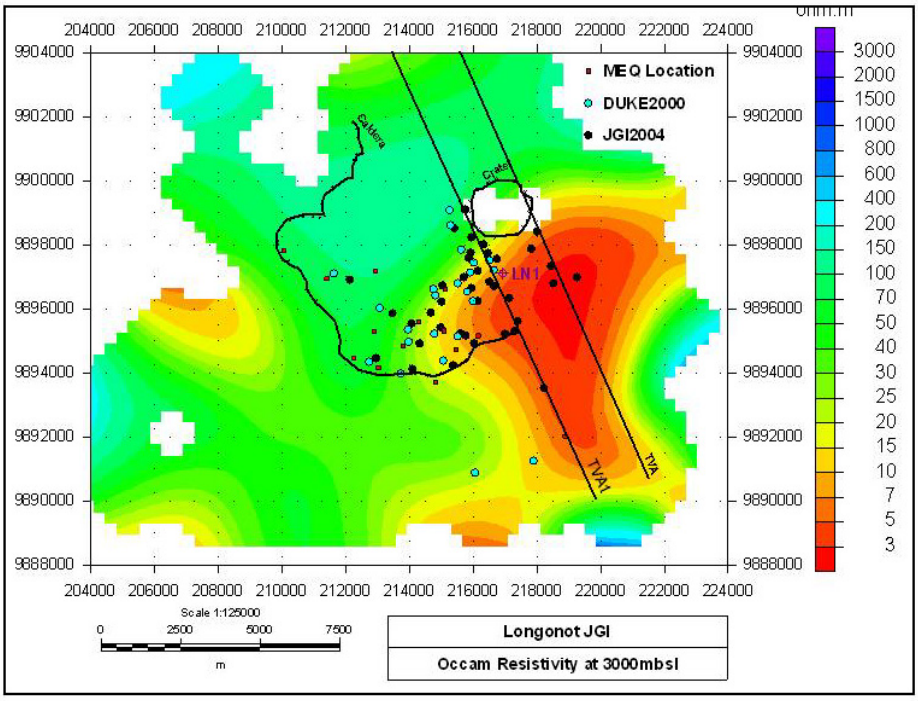

Figure 12: Resistivity at 3000 mbsl showing the location of MEQ in relation to Longonot crater, caldera and an interpreted Tectonic Volcanic Axis (TVA). MEQ occur on the boundary of the deep low resistivity and high resistivity.

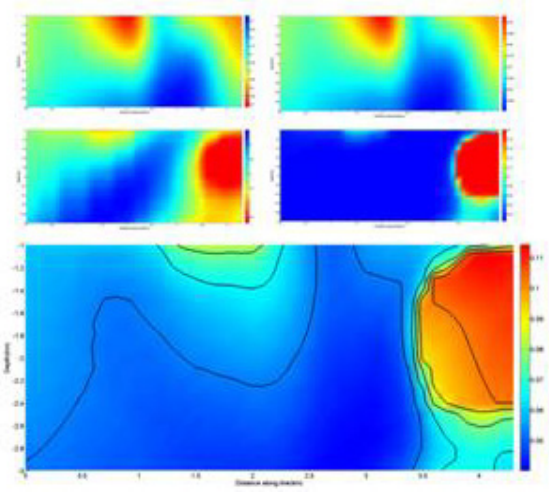

Figure 13: 2D sections showing resistivity, P-wave velocity, associated derived porosity and the porosity distribution using a weighted mean function.

4. DRILLING STRATEGY FROM RESULTS OF JGI

From the results of the JGI, we have inferred that the combined use of MEQ and MT data can be used to successfully locate high production wells. The S-wave splitting and MT polarization can be very useful if MEQ stations are deployed appropriately. The combination of MEQ and MT is useful even if only a few MEQ are recorded. The complementary data provided by both MT and MEQ especially in response to anisotropy and heterogeneity caused by fluid-filled fractures can be used to target drilling directions for both exploration and production wells. These studies are useful in areas that might not have any surface manifestations or traces of exposed fractures and faults. The best drilling targets are along the buried, probably older fractures that might have been reactivated. This might a preferred strategy rather than routinely drilling across surface traces of fractures.

5. CONCLUSIONS

The joint interpretation of MEQ and MT data can be a very powerful tool for exploration and optimizing production in existing fields. The analysis and understanding of the complex fluid flow regimes and targets for drilling can be achieved by a joint imaging scheme that resolves structural anisotropy which is associated with aligned fluid-filled fractures.

ACKNOWLEDGEMENTS

We are grateful to the United Nations Environmental programme (UNEP) and the Global Environmental Facility (GEF) for the initial support of JGI and development of new equipment for increased geothermal exploration. We are also grateful to KenGen, Landsvirjkun and the Icelandic geological survey (ISOR). Continued development of JGI is supported by the Auckland University, New Zealand.

REFERENCES

Christensen, N., and Wilkens, R. (1982). Seismic properties, density, and composition of the Icelandic crust near Reydarfjordur. J. Geophys.Res., 87, 6389-6395.

Crampin, S., and Peacock, S. (2005). A review of shear-wave splitting in the compliant crack-critical anisotropic Earth. Wave Motion, 41(1), 59-77.

Flovenz, O. G. (1985). Application of Subsurface Temperature-Measurements in Geothermal

Prospecting in Iceland. Journal of Geodynamics, 4(1-4), 331-340

Malin, P., Leary, P., Shalev, E., and Onacha, S.,: Joint Geophysical Imaging of Poroperm Distributions in Fractured reservoirs, *Proceedings* of the annual Geothermal Resources Council meeting, Reno, Nevada (2009).

Onacha, S.A. (2006). Hydrothermal fault zone mapping using seismic and electrical measurements. Ph.D Thesis, Duke University pp225

Onacha, S., Malin, P., Shalev, E., Cumming, W., Arnasson, K., and Palsson, B.: Formulation of a porosity operator for joint interpretation of resistivity and microearthquake data across a fluid-filled fracture zone, *Proceedings* of the annual New Zealand Geothermal workshop, Auckland, NZ (2007)

Onacha, S., Malin, P., Shalev, E., Simiyu, S., and Cumming, W.: B.: Microearthquake and resistivity imaging of the Longonot geothermal prospect, Kenya. *Proceedings* of the annual New Zealand Geothermal workshop, Auckland, NZ (2007).

Onacha, S., Shalev E., Malin, P., and Leary, P.: Joint Geophysical Imaging of fluid-filled fracture zones in Geothermal Fields in the Kenya Rift Valley. Accepted for proceedings of the Geothermal Resources Council in Reno, Nevada, USA (2009).

Simpson, F., and Bahr, K: Practical Magnetotellurics. Cambridge University Press

Waldhauser, F., and Ellsworth, W.L., A double-difference earthquake location algorithm: method and application to the Northern Hayward Fault, California, Bulletin of the Seismological Society of America, 90, (2000), 1353-1368.

Wyllie, R., Gregory, A., and Gardner, G. (1958). An experimental investigation of factors affecting elastic wave velocities in porous media. Geophysics, 23, 459-493.